Vibrational Feshbach resonances in dissociative electron attachment to uracil

Gordon A. Gallup and Ilya I. Fabrikant

Phys. Rev. A **83**, 012706 — Published 18 January 2011

DOI: 10.1103/PhysRevA.83.012706

Vibrational Feshbach resonances in dissociative electron attachment to uracil

Gordon A. Gallup[1] and Ilya I. Fabrikant[1,2]

[1] *Department of Physics and Astronomy, University of Nebraska, Lincoln, Nebraska 68588-0299, USA*

[2] *Department of Physics and Astronomy, The Open University, Walton Hall, Milton Keynes MK7 6AA, UK*

Abstract

Low-energy dissociative electron attachment to uracil molecules in the gas phase is partly controlled by interaction between the lowest σ^* resonance with a dipole-supported anion state. We calculate this contribution using a combination of the finite element discrete model with the resonance R-matrix theory. Deuterated uracil is investigated, also, and a strong isotope effect is found. The results agree qualitatively and semiquantitatively with experimental data, but for a complete description of the process the interaction between a second N—H bond σ^* resonance in the molecule and the second π^* resonance should be included.

PACS numbers: 34.80.Ht

I. INTRODUCTION

An interesting feature of the dissociative electron attachment (DEA) process is that low-energy electrons may not only dissociate the molecular target, but may do so at well defined reaction sites often leading to almost 100% bond selectivity[1], thence initiating controlled chemical processing in the local environment. This feature is particularly important in DEA to biological molecules because of the recently discovered role of the DEA process in radiation damage [2].

The most abundant product of DEA to the building blocks (purines and pyrimidines) of DNA is the dehydrogenated closed-shell anion $[M\text{-}H]^-$[3]. A series of sharp peaks in DEA cross sections to uracil [1, 4–9], thymine [10] and adenine [11] were identified [5] as vibrational Feshbach resonances (VFRs) [12]. The lowest $^2\Sigma$ anion state is strongly antibonding between N_1 and H. (The subscripts here and below refer to the atom location, see Fig. 1). It was therefore argued that this state drives low-energy DEA in uracil leading to production of the $(U\text{-}H)^-$ anion and H atom. In addition, due to the large dipole moment of uracil, $\mu = 4.7$ D, an electron can be captured by the dipolar field with simultaneous vibrational excitation leading to VFRs.

VFRs in uracil and thymine arise wholly from the ejection of a hydrogen atom residing on a nitrogen rather than from a carbon atom, Fig. 1. The experimental proof was provided first for thymine by Abdoul-Carime *et al* [13]. Using thymine deuterated only at the carbon positions, their mass analysis showed that only $[M\text{-}H]^-$ appeared below electron energies of 4 eV, and there was no contribution from $[M\text{-}D]^-$. Moreover, the observed yield was essentially the same as for the undeuterated thymine. Ptasinska *et al* [1] confirmed these observations for the uracil molecule and, in addition, showed that the sharp structure in the cross section appears due to H loss from N_1-H whereas H loss from the N_3-H site is completely suppressed below 1.4 eV. When the uracil molecule was methylated at the N_1 position, that is, the H atom was replaced by the CH_3 radical at the N_1 site, no $[M\text{-}H]^-$ anions were observed below 1.4 eV. If, on the other hand, the uracil was methylated at the N_3 position, the sharp feature at 1.0 eV was preserved, whereas the cross section was lower and had different shape at higher energies.

More detailed studies for thymine were performed by Burrow *et al* [9] and Denifl *et al* [3]. In particular Burrow *et al* [9] noticed that the σ_1^* valence orbital is also strongly

antibonding between N_1 and C_6 atoms which leads to excitation of the C_6-H and N_1-C_6 stretching vibrations. Indeed, additional structure corresponding to $n_1\nu(N_1H)n_2\nu(N_1C_6)$ and $n_1\nu(N_1H)n_2\nu(C_6-H)$ overtones was observed in the DEA cross sections.

Uracil deuterated at the N_1 and N_3 positions was examined by Scheer *et al* [8] who reported the total anion yield, that is, without mass analysis. Although the electron energy resolution was poorer, the shape of the yield in uracil was consistent with that seen by others. In particular, two VFRs at 0.69 and 1.01 eV were observed in nondeuterated uracil. It was also noted that a broader peak at 1.7 eV was coincident with the location of the second $^2\Pi$ resonance. In the N-deuterated uracil, on the other hand, no evidence for sharp VFRs was found and only a broad peak at 1.16 eV was observed. These data were evidence for a substantial isotope effect and implied that the reduced tunneling rate of a deuterium atom relative to that of hydrogen gave rise to VFRs that were too narrow to be observed with the resolution employed.

Although no other studies of N-deuterated uracil have been reported, Denifl *et al* [3] have subsequently studied N-deuterated thymine with high electron energy resolution and mass selectivity. They found a strong isotope effect in N-deuterated thymine whereas the DEA cross section for the C-deuterated thymine was practically indistinguishable from that for thymine. Moreover, it was found that all narrow vibrational Feshbach resonances are due to the H loss from the N_1 site whereas a broader asymmetric peak near 2 eV is due to the interaction between the second lowest π^* resonance with the second σ^* resonance. The isotope effect was the most pronounced in the H loss from the N_1 site. In this case the cross section for thymine was reduced by a factor of 40, whereas for the H loss from the N_3 site the cross section was reduced by a factor of 20.

These observations allow us to conclude that the problem of the $[M\text{-}H]^-$ formation, where M stands for uracil or thymine, can be separated into two parts. The H loss from the N_1 site can be treated as a direct capture into the lowest σ^* unoccupied orbital assisted by the interaction with the dipole-supported states. The H loss from the N_3 site should be treated as capture into the second unoccupied π^* orbital with the following transition into the second σ^* state due to vibronic coupling. In the latter case the DEA mechanism is similar to that observed previously for chlorobenzene and vinyl chloride [14] and calculated for acetylene [15]. Although it is hard to separate these two reaction channels in practice, information about the cross section for the first reaction can be provided by performing

experiments with uracil or thymine methylated at the N_3 position [1].

Calculation of cross sections for these two channels involves different physics, and therefore requires different methods. The H loss from the N_1 site involves a broad σ^* shape resonance and VFRs, and therefore requires the nonlocal approach [16], or equivalent R-matrix approach [17]. On the other hand, the H loss from the N_3 site is primarily due to the relatively narrow π^* resonance, and the local approximation is adequate in this case. Unfortunately, the necessary inclusion of the vibronic coupling between σ^* and π^* resonances makes this problem more complicated.

Ab initio calculations[18–20] of the eigenphase sums for electron-uracil scattering indicate, in addition to the π^* resonances, only narrow σ^* resonances of Feshbach type at higher energies [20]. No broad shape resonances were reported. Note, however, that Winstead and McKoy [19] detected a broad peak in the partial A' cross section centered around 8.5 eV that "is likely real and due to one or more C-H or N-H σ^* shape resonances". The situation here is similar to that observed in hydrogen halides [21–24] and discussed recently for formic acid [25, 26]: the width of the lowest σ^* resonance is so large, that the resonance is difficult to discern in the scattering eigenphase sum or the partial cross section. For determination of the resonance parameters the scattering phase shift should be decomposed into the resonance and background phase shifts. The latter is dominated by the strong dipolar and polarization interactions leading to a decrease of the total phase shift as a function of energy. This decomposition can be accomplished by combining the finite element discrete model (FEDM) [27] with the resonance R-matrix theory [17].

In the present paper we calculate the DEA cross section for uracil involving the H loss from the N_1 site. Our approach to this problem is similar to that used in DEA calculations for formic acid [25]. We calculate the potential curve and the width function for the σ^* resonance along the reaction coordinate N_1-H using FEDM, and then obtain the resonance R-matrix parameters which reproduce the calculated width. With these parameters we calculate the DEA cross sections. Since the model is one-dimensional, our calculations are unable to reproduce structures due to $n_1\nu(N_1H)n_2\nu(N_1C_6)$ and $n_1\nu(N_1H)n_2\nu(C_6-H)$ overtones [9].

II. INPUT DATA

We represent the energy of the N_1-H stretch by an effective one-dimensional potential in the Morse form

$$V(\rho) = A[\exp(-\alpha\rho) - 1]^2 \tag{1}$$

where $\rho = R - R_e$ is the reaction (N_1-H) coordinate relative to the equilibrium separation R_e. The Morse parameters were chosen to fit *ab initio* calculations. We obtained $\alpha = 0.95345$ a.u., $A = 0.28698$ a.u. The corresponding energy of the first vibrationally excited state is 0.451 eV, somewhat higher but close to the experimental value 0.432 eV [28], To reproduce this value, our curve has been adjusted by changing the value of parameter α to 0.9110 a.u.

The R-matrix pole representing the anion curve is parametrized in the form

$$U(\rho) = B\exp(-2\beta\rho) - C\exp(-\beta\rho) + D, \tag{2}$$

and the R-matrix surface amplitude $\gamma(\rho)$ as

$$\gamma(\rho) = \gamma_1 + \frac{\gamma_2}{e^{\zeta\rho} + a}. \tag{3}$$

The parameters in these equations were fitted to reproduce the results of *ab initio* calculations of the anion resonance energy and the resonance width Γ. The relation between the resonance energy U_r and the position of the R-matrix pole is

$$U_r(\rho) = U(\rho) + \Delta(E_r(\rho))$$

where the electron resonance energy $E_r(\rho) = U_r(\rho) - V(\rho)$, and the resonance shift $\Delta(E)$, as well as the resonance width $\Gamma(E)$, are calculated according to standard equations of the R-matrix theory [29]. In practice we calculate $U(\rho)$ from *ab initio* values of $U_r(\rho)$ and fit parameters in Eqs. (2), (3) to the obtained values of $U(\rho)$ and $\Gamma(\rho, E)$. We found that this procedure is very insensitive to the parameter D. Unfortunately, this parameter, to some extent, controls the crossing point between the potential curves, and the DEA cross section is very sensitive to this parameter. We investigated how the DEA cross section depends on D by taking two values of this parameter: $D = -0.001467$ a.u. (model 1), $D = -0.02$ a.u. (model 2). In addition we tried $D = 0.03655$ a.u., approximately corresponding to the 0.8 eV reaction threshold calculated by Hanel *et al* [4]. However, in this case we were unsuccessful in obtaining a good fit. Although the asymptotic value of the anion energy $D = 0.03655$ a.u.

might be realistic, our parametrization is not flexible enough to provide adequate repulsion in the Franck-Condon region in this case. In each case we adjust parameters B and C in order to reproduce the *ab initio* calculated anion curve in the Franck-Condon region. The potential energy curves for models 1 and 2 are presented in Fig. 2. We also present there the curve corresponding to the dipole-supported state for model 1.

The long-range electron-molecule interaction outside the R-matrix sphere was modelled by a combination of the dipolar potential and polarization potential. The dipole moment function $\mu(R)$ was calculated using the GAMESS computation package[30] with a 6-311G(d) basis. The N_1—H (see Fig. 1) bond distance was held at a series of fixed distances while the geometry of the remaining atoms was relaxed to minimize the total energy. In the range of internuclear distances important for our calculations the function $\mu(R)$ is linear, and with good accuracy can be approximated as

$$\mu(R) = \mu_0 + 0.43765(R - R_0) \tag{4}$$

where $R_0 = 1.89$ a.u. is the equilibrium N_1-H separation and $\mu_0 = 1.867$ a.u. is the corresponding dipole moment.

We also calculated the polarizability tensor α_{ij} at the equilibrium internuclear separation. In the reference frame where the N_1 atom has xyz coordinates (-0.97468,1.16671,0) Å, and the C_2 atoms coordinates (0.39804,1.20645,0) Å, the components of the polarizability tensor are, in Å^3, $\alpha_{xx} = 8.15102$ $\alpha_{xy} = -0.59070$, $\alpha_{yy} = 10.76421$, $\alpha_{zz} = 3.40731$, and $\alpha_{xz} = \alpha_{yz} = 0$. We have transformed this tensor into the reference frame with the z axis along the molecular dipole moment (see Fig. 1) and averaged it over the electron density distribution corresponding to the lowest dipolar angular function [31]. The result is 7.8045 Å^3 = 52.73 a.u., not very different from the mean value $\bar{\alpha} = 7.44085$ obtained from the average over the isotropic distribution.

The FEDM[27] method provided an *ab initio* determination of the $\Gamma(\rho, E)$ function. Briefly, one approximates the continuum wave function with a sequence of discrete (L^2) functions and applies the Fano configuration interaction procedure[32] to find the lifetime amplitude and then Γ. Typically, 30 to 60 single Gaussians are used, in this case mixing s and p symmetries. The single particle kinetic energies of these ranged from 0.01 to ≈ 50 eV; however, the results are not sensitive to these limits. Uracil has a dipole moment substantially above the critical value, producing at least one dipole bound state, but no

attempt was made to add functions to reproduce this state more accurately. The equilibrium geometry of the uracil negative ion was determined under the constraints of planarity and a number of fixed N—H distances at N_1, but allowing the in-plane bond angle to relax. The resulting $\Gamma(\rho, E)$ function at each distance does have the finite $\Gamma(E \to 0)$ threshold behavior expected of super-critical dipole systems.[33] The fitting procedure results in an R-matrix width, and in Fig. 3 we present a comparison with the *ab initio* calculated $\Gamma(\rho, E)$. The R-matrix width includes the long-range electron interaction with the molecular dipole moment whereas in the FEDM calculations these effects are not included to a full extent. This explains the disagreement between the two calculations in the low-energy region.

III. RESULTS AND DISCUSSION

A. DEA cross sections for uracil

In Fig. 4 we present the DEA cross section calculated with the parameters of model 1 (note semilog scale). Very pronounced VFRs are seen, particularly two resonances below the $v = 2$ and $v = 3$ thresholds. We demonstrate the cross section behavior below the $v = 3$ threshold in more detail in Fig. 5 where we plot cross section as a function of $-\log_{10}(E_t - E)$ where $E_t = 1.25778$ eV is the threshold energy.

Apparently this is the first case when two VFRs in DEA are produced near the same vibrational threshold. This occurrence is due to the high dipole moment of uracil. According to the general theory [33], for molecules with supercritical dipole moments, $\mu > \mu_{cr} = 0.6395$ a.u., the binding energies of dipole-supported states form a geometric progression of the type

$$E_n = E_0 \exp(-2\pi n/\tau), \qquad n = 0, 1, ... \tag{5}$$

where E_0 is the energy of the lowest state, and τ is a parameter depending only on the molecular dipole moment. For μ close to μ_{cr} the parameter τ is small and the common ratio E_{n+1}/E_n is small exponentially, and in this case almost all, or even all, dipole-supported states are destroyed by rotations [33]. For example, HF and water molecules do not bind an electron at all, although their dipole moment is supercritical. For uracil $\tau = 1.967$ and the common ratio $E_{n+1}/E_n = 0.00395$. The computed resonance positions below the $v = 2$ threshold agree very well with this value, although a certain deviation is observed at the $v = 3$ threshold where the computed value of E_1/E_0 is 0.0053. This is caused by the

interchannel interaction which almost completely destroys the lowest resonance at the $v = 4$ threshold. This can be seen from Fig. 2 which indicates that the position of the $v = 3$ state is close to the crossing point whereas the position of the $v = 4$ state is above it.

For the purpose of comparison with experiment we have averaged the theoretical cross section over a Gaussian distribution of width 0.07 eV (dashed curve in Fig. 4 and curve 1 in Fig. 6).

The resulting cross section differs in several aspects from that measured[1, 4–9]. First, the $v = 2$ resonance is not visible on the linear scale. Second, the major peak occurs at $E = 1.196$ eV instead of the observed peak position $E = 1.01$ eV [8]. Third, the peak value of the cross section, $\sigma_{peak} = 0.034 \times 10^{-16}$ cm^2 is substantially higher than the experimental estimate of Aflatooni *et al* [7], 0.0044×10^{-16} cm^2. On the other hand, the Innsbruck group [6] gives 0.16×10^{-16} cm^2, 4.7 times bigger than the theory. Thus the theoretical value lies between two experimental measurements. Note that the peak value strongly depends on the instrumental width. When we increase it to 0.1 eV the peak cross section drops to 0.027×10^{-16} cm^2.

We can modify the theoretical results in two ways. First, we can try to reduce the DEA cross section by increasing the parameter D in Eq. (2). However, our attempts to do this led to disappearance of the major peak below the $v = 3$ threshold. On the other hand, we can enhance the $v = 2$ peak by reducing the parameter D (model 2).

To understand the disagreement in the position of the major peak, we have calculated the binding energy E_0 of the dipole-supported state at the equilibrium internuclear separation with the R-matrix parameters employed in our model 1. This results in $E_0 = 37.8$ meV, more than a factor of 2 smaller than the measured value [34, 35]. The value of the binding energy can be changed by varying R-matrix parameters responsible for the short-range interaction or by increasing the strength of the long-range interaction. Variation of the R-matrix parameters in order to increase the binding energy led to a width function very different from the results of *ab initio* calculations, therefore we abandoned this approach and increased by 5.3% the dipole moment instead. In addition, we increased the average polarizability to 83 a.u. As a result, the binding energy has grown to 87.3 meV, very close to experiment.

Results of these three calculations (model 1, model 2 and modified model 1) folded with a Gaussian beam profile of width 0.07 eV are presented in Fig. 6. In the calculation of model

2, the VFR below the $v = 2$ threshold becomes visible in the averaged cross section on the linear scale, and the overall structure becomes similar to that observed [8]. The magnitude of the cross section at the peak increases further to 0.115×10^{-16} cm^2 but remains lower than the experimental value of Feil *et al* [6]. In the calculation of modified model 1, the peak's position goes down to 1.132 eV which is still higher by 0.12 eV than the experimental result.

In Fig. 7 we present results for the modified model 1 together with experimental DEA cross sections for uracil and uracil methylated at the N_3 position[1]. The experimental cross sections are normalized arbitrarily, but their relative values are given as in Ref. [1], so it is clearly seen that the experimental signal below $E = 1.4$ eV is due to the H loss from the N_1 site. Agreement of the theoretical curves with experimental cross sections for uracil remains more qualitative than quantitative. This may be expected for a such a complex target, particularly in view of the numerous approximations made in the calculations.

Since the DEA cross section depends very strongly on the initial vibrational state, an increase of vibrational temperature can lead to a substantially higher cross sections than those calculated for $v = 0$. To investigate this effect, we have calculated DEA cross section for $T = 300$ and 450 K (the temperature in experiment [3]), and did not find a significant effect. However, a further temperature increase produces a noticeable enhancement at low electron energies. To demonstrate this, we present comparison of the $T = 0$ K results with $T = 723$ K results in Fig. 8. Note that the $T = 300$ K cross section does not differ at all from that for $T = 0$. At $T = 723$ K we see a strong enhancement of the cross section in the low-energy region, particularly of the $v = 2$ peak. However, the cross section in this region is still very small compared to the value of the major peak at the $v = 3$ threshold.

B. Deuterated uracil and isotope effect

In Fig. 9 we present the DEA cross section for the N-deuterated uracil calculated with the parameters of model 1. The reduced mass in these calculations was increased by 2. Accordingly, for low-lying vibrational states, the vibrational frequency has decreased by $1/\sqrt{2}$. Since the temperature effect is more substantial for the deuterated uracil, we also show cross sections for DEA from the first two vibrationally excited states. Several VFRs, including those below the $v(N_1 - D) = 2, 3, 4$ and 5 and thresholds are observed. Some

resonances demonstrate the double feature described by Eq. (5), as discussed above for nondeuterated uracil.

Because the existing experimental data for N-deuterated uracil [5] had insufficient resolution to observe the VFRs, we compare our calculated results with the measurements of Denifl *et al* [3] for N-deuterated thymine. The $(M\text{-}H)^-$ yield in uracil and thymine are quite close, although VFRs in thymine appear to be somewhat more visible than in uracil.

In Fig. 10 we present comparison of the experimental results with calculations of model 1 for two vibrational temperatures. One has to go to temperatures above 700K to see substantial effects on DEA cross sections. This is demonstrated by presenting results for $T = 0$ and $T = 723$ K. The temperature effect leads to a significant enhancement of the $v = 4$ peak and improves agreement with experiment. However, for the experimental temperature $T = 450$ K the effect is small. In addition the theoretical results suffer from the same discrepancy found in the nondeuterated case: the position of the major peak is substantially higher, by about 0.27 eV, than the experimental position. A more careful analysis shows that the main theoretical peak occurs below the $v = 5$ threshold whereas the observed peak occurs below the $v = 4$ threshold. As is apparent from Fig. 9, the peaks occur below each vibrational excitation threshold, but their magnitude varies strongly with v. The value of v corresponding to the maximum cross section strongly depends on the position of the crossing point between the neutral and anion curve, Fig. 2. To demonstrate this, in Fig. 11 we present comparison of cross sections, calculated with model 1, and model 1 with the anion curve shifted by the amount $\Delta U = -0.005$, -0.007, and -0.009 a.u. In the calculation with $\Delta U = -0.007$ a.u. the $v = 4$ peak becomes as pronounced as the $v = 5$ peak, and in the calculation with $\Delta U = -0.009$ a.u.$= -0.245$ eV the $v = 4$ peak becomes dominant, and the curve agrees very well with the experiment. This last adjustment represents moving approximately 75% of the way from $\nu = 5$ to $\nu = 4$ and demonstrates that threshold peaks are very sensitive to the crossing point. Here the experimental measurements can serve as a tool for the determination of its location.

We note the striking mass effect on the absolute magnitude of the cross section for the H/D loss from the N_1 site: the peak value is reduced by a factor of 20. This is typical for hydrogen halides[23]. For thymine Denifl *et al*[3] observed an even higher reduction by a factor of 40.

IV. CONCLUSION

Because of the complexity of DEA in uracil and thymine, it is important to explore different mechanisms contributing to this process. In the present paper we have investigated the role of the broad σ^* N_1-H shape resonance and its interaction with the dipole-supported anion in uracil leading to VFRs in the DEA H loss from the N_1 site. Because of the substantial contribution of the second π^* resonance not included in the present calculations, the comparison with experiment can be done only qualitatively rather than quantitatively. However, the major features of the process are reproduced by comparing the calculated results with the DEA for uracil methylated at the N_3 site. Calculations for the deuterated uracil demonstrate a significant vibrational temperature effect in the low-energy region and a strong isotope effect. The latter confirms experimental observations [3].

The position of the major VFR is somewhat too high, by 0.1-0.2 eV as compared with the experimental position. For deuterated uracil we find a strong dependence of the peaks position on the crossing point, therefore experimental measurements can serve as a tool for determination of its location.

We expect that more accurate calculations of the input parameters will lead to a better agreement. The major task for future studies is incorporation of the $\sigma^* - \pi_2^*$ coupling leading to the loss of H from the N_3 site.

Acknowledgments

The authors are grateful to P. D. Burrow for many stimulating discussions and valuable comments on the preliminary version of the manuscript, and to P. Scheier for providing experimental data on thymine in numerical form. This work was supported in part by the National Science Foundation under Grant No. PHY-0652866, and by a Marie Curie International Incoming Fellowship (FP7-PEOPLE-2009-IIF-252714).

---

[1] S. Ptasinska, S. Denifl, P. Scheier, E. Illenberger, and T. D. Märk, Angew. Chem. Int. Ed. **44**, 6941 (2005).

[2] L. Sanche, Eur. Phys. J. D **35**, 367 (2005).

[3] S. Denifl, P. Sulzer, F. Zappa, S. Moser, B. Kräutler, O. Echt, D. K. Bohme, T. D. Märk, and P. Scheier, Int. J. Mass Spectrom. **277**, 296 (2008).

[4] G. Hanel, B. Gstir, S. Denifl, P. Scheier, M. Probst, B. Farizon, M. Farizon, E. Illenberger, and T. D. Märk, Phys. Rev. Lett. **90**, 188104 (2003).

[5] A. M. Scheer, K. Aflatooni, G. A. Gallup, and P. D. Burrow, Phys. Rev. Lett. **92**, 068102 (2004).

[6] S. Feil, K. Gluch, S. Matt-Leubner, P. Scheier, J. Limtrakul, M. Probst, H. Deutsch, K. Becker, A. Stamatovic, and T. D. Märk, J. Phys. B **37**, 3013 (2005).

[7] K. Aflatooni, A. M. Scheer, and P. D. Burrow, Chem. Phys. Lett. **408**, 426 (2005).

[8] A. M. Scheer, C. Silvernail, J. A. Belot, K. Aflatooni, G. A. Gallup, and P. D. Burrow, Chem. Phys. Lett. **411**, 46 (2005).

[9] P. D. Burrow, G. A. Gallup, A. M. Scheer, S. Denifl, S. Ptasinska, T. Märk, and P. Scheier, J. Chem. Phys. **124**, 124310 (2006).

[10] S. Denifl, S. Ptasinska, M. Probst, J. Hrusak, P. Scheier, and T. D. Märk, J. Phys. Chem. A **108**, 6562 (2004).

[11] H. D. Flosadottir, S. Denifl, F. Zappa, N. Wendt, A. Mauracher, A. Bacher, H. Johnsson, T. D. Märk, P. Scheier, and O. Ingolfsson, Angew. Chem. Int. Ed. **46**, 8057 (2007).

[12] H. Hotop, M.-W. Ruf, M. Allan, and I. I. Fabrikant, Adv. At. Mol. Phys. 49, 85 (2003)

[13] H. Abdoul-Carime, S. Gohlke, and E. Illenberger, Phys. Rev. Lett. **92**, 168103 (2004).

[14] K. L. Stricklett, S. C. Chu and P. D. Burrow, Chem. Phys. Lett. **131**, 279 (1986).

[15] S. T. Chourou and A. E. Orel, Phys. Rev. A **77**, 042709 (2008).

[16] W. Domcke, Phys. Rep. **208**, 97 (1991).

[17] I. I. Fabrikant, Phys. Rev. A **43**, 3478 (1991).

[18] F. A. Gianturco and R. R. Lucchese, J. Chem. Phys. **120**, 7446 (2004).

[19] C. Winstead and V. McKoy, J. Chem. Phys. **125**, 174304 (2006).

[20] A. Dora, J. Tennyson, L. Bryjko and T. van Mourik, J. Chem. Phys. **130**, 164307 (2009).

[21] I. I. Fabrikant, S. A. Kalin and A. K. Kazansky, J. Phys,. B **25**, 2885 (1992).

[22] J. Horáček and W. Domcke, Phys. Rev. A **53**, 2262 (1996).

[23] G. A. Gallup, Y. Xu and I. I. Fabrikant, Phys. Rev. A **57**, 2596 (1998).

[24] M. Čižek, J. Horaček, and W. Domcke, Phys. Rev. A **60**, 2873 (1999).

[25] G. A. Gallup, P. D. Burrow and I. I. Fabrikant, Phys. Rev. A **79**, 042701 (2009).

[26] I. I. Fabrikant, J. Phys.: Conf. Series, **204**, 012004 (2010).

[27] R. K. Nesbet, Phys. Rev. A **24**, 1184 (1981).

[28] P. Colarusso, K. Zhang, B. Guo, and P. F. Bernath, Chem. Phys. Lett. **269**, 39 (1997).

[29] A. M. Lane and R. G. Thomas, Rev. Mod. Phys. **30**, 257 (1958).

[30] M. W. Schmidt, K. K. Baldridge, J. A. Boatz, S. T. Elbert, M. S. Gordon, J. H. Jensen, S. Koseki, N. Matsunaga, K. A. Nguyen, S. J. Su, T.L.Windus, M. Dupuis, and J. A. Montgomery, J. Comput. Chem. **14**, 1347 (1993).

[31] M. H. Mittleman and R. E. von Holdt, Phys. Rev. **140A**, 726 (1965); I. I. Fabrikant, Sov. Phys. JETP **44**, 77 (1976).

[32] U. Fano, Phys. Rev. **124**, 1866 (1961).

[33] I. I. Fabrikant, J. Phys. B **16**, 1253 (1983).

[34] J. H. Hendricks, S. A. Lyapustina, H. L. de Clercq, J. T. Snodgrass, and K. H. Bowen, J. Chem. Phys. **104**, 7788 (1996).

[35] J. Scheidt, R. Weinkauf, D. M. Neumark, and E. W. Schlag, Chem. Phys. **239**, 511 (1998)

FIG. 1: Molecular structure of uracil (U), uracil methylated at the N_3 position (3mU), and thymine (T). The arrow indicates the direction of the dipole moment in uracil.

FIG. 2: (Color online) Potential energy curves as functions of the N_1-H distance relative to equilibrium. Note that the equilibrium position is $R_e = 1.890$ a.u.= 0.9995 Å. The two anion curves are R-matrix poles for models 1 (dashed curve) and 2 (solid curve). Circles are corresponding energies from FEDM calculations. Dotted curve: adiabatic anion curve for model 1. Horizontal lines indicate the positions of vibrational energy levels of the neutral.

FIG. 4: (Color online) DEA cross sections for uracil, model 1. Solid curve, nonaveraged cross sections. Dashed curve, cross sections folded with a Gaussian distribution of width 0.07 eV. The vibrational excitation thresholds are indicated by arrows.

FIG. 5: (Color online) DEA cross sections for uracil below the $v = 3$ threshold plotted as a function of $-\log_{10}(E_t - E)$ where $E_t = 1.25778$ eV is the threshold energy and E is the electron energy in eV.

FIG. 6: (Color online) A comparison of the folded DEA cross sections for models 1 (curve 1), 2 (curve 2) and modified model 1 (curve 1m).

FIG. 7: (Color online) The folded DEA cross section calculated with the modified model 1 (dashed line). Experimental data: curve 1, measured negative ion yield for uracil; curve 2, measured negative ion yield for uracil methylated at the N_3 position. See text about normalization of experimental curves.

FIG. 8: (Color online) DEA cross section calculated for vibrational temperatures $T = 0$ (solid curve) and $T = 723$ K (dashed curve).

FIG. 3: (Color online) Resonance width as a function of energy for three internuclear N_1-H distances (given in the same units as in Fig. 2). FEDM calculations: dashed curves; R-matrix parameter fit: solid curves.

FIG. 9: (Color online) DEA cross sections for deuterated uracil calculated for three initial vibrational states, $v_i = 0$ (bottom curve), $v_i = 1$ (middle curve), and $v_i = 2$ (top curve) with the parameters of model 1. The vibrational excitation thresholds for the $v_i = 0$ initial state are indicated by arrows.

FIG. 10: (Color online) DEA cross sections for deuterated uracil averaged over a Gaussian distribution of width 0.07 eV. Solid curve, model 1, $T = 0$; dashed curve, model 1, $T = 723$ K. Curve 'exp', arbitrarily normalized deconvoluted ion yield in experiment [3] for thymine.

FIG. 11: (Color online) DEA cross sections for deuterated uracil averaged over a Gaussian distribution of width 0.07 eV. Curve 1: model 1; curve 2, 3, and 4: model 1 with the anion potential curve shifted down by 0.005, 0.007, and 0.009 a.u. respectively.

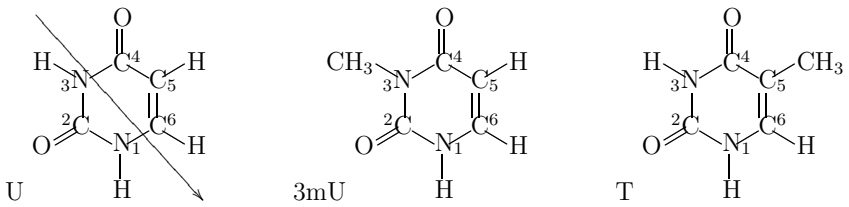

Figure 1: Molecular structure of uracil (U), uracil methylated at the N_3 position (3mU), and thymine (T).

Figure 1 AY10442 16Dec2010

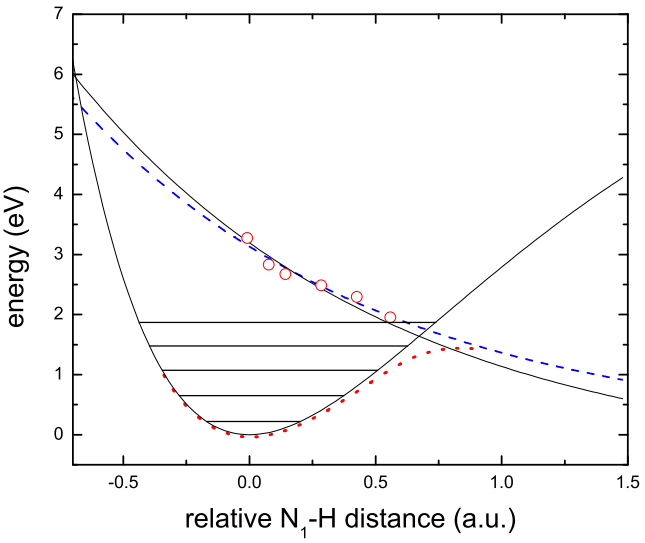

Figure 2 AY10442 16Dec2010

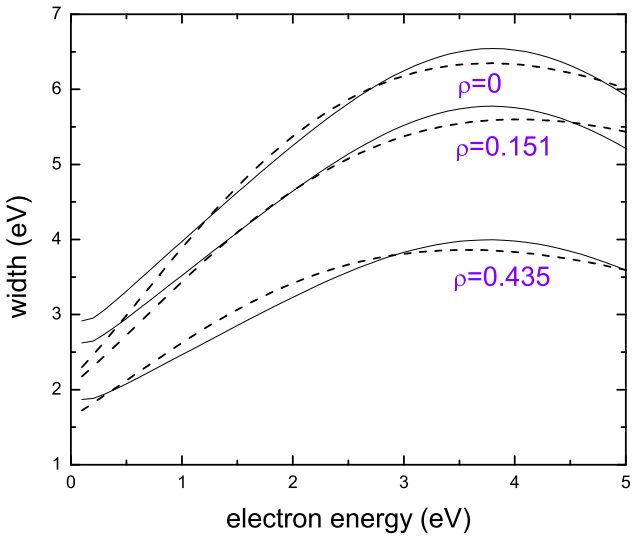

Figure 3 AY10442 16Dec2010

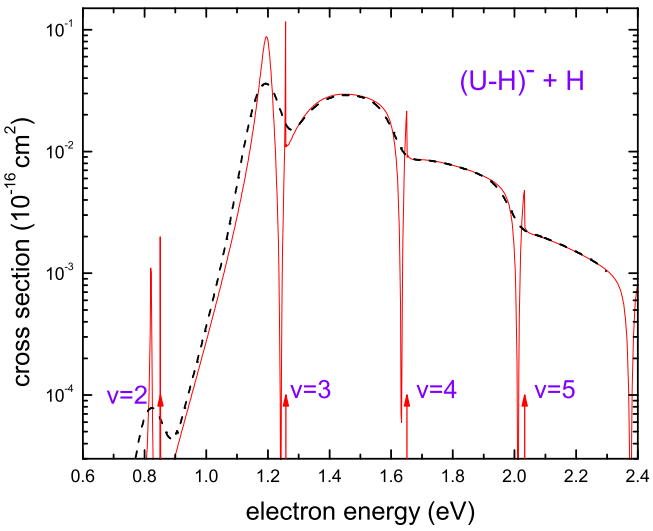

Figure 4 AY10442 16Dec2010

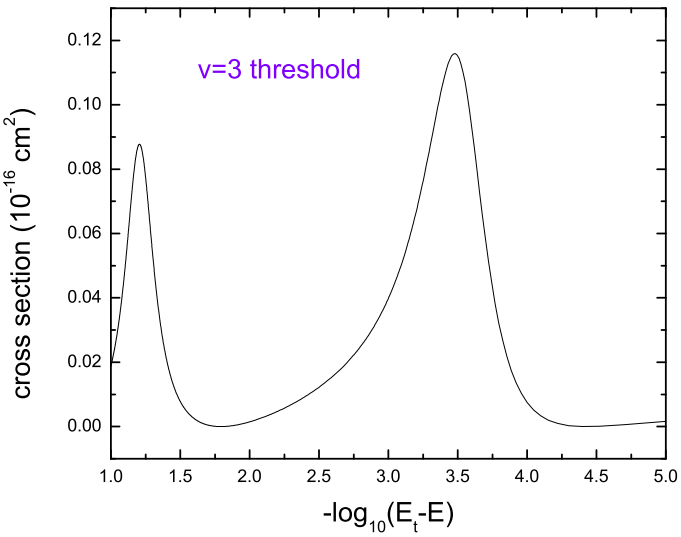

Figure 5 AY10442 16Dec2010

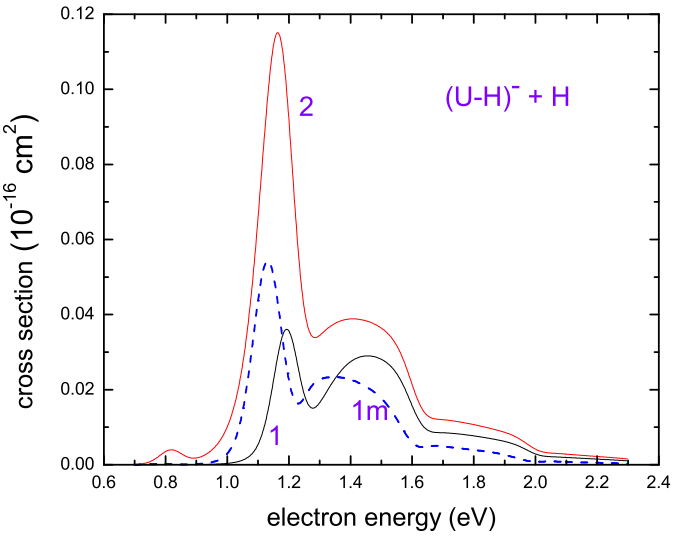

Figure 6 AY10442 16Dec2010

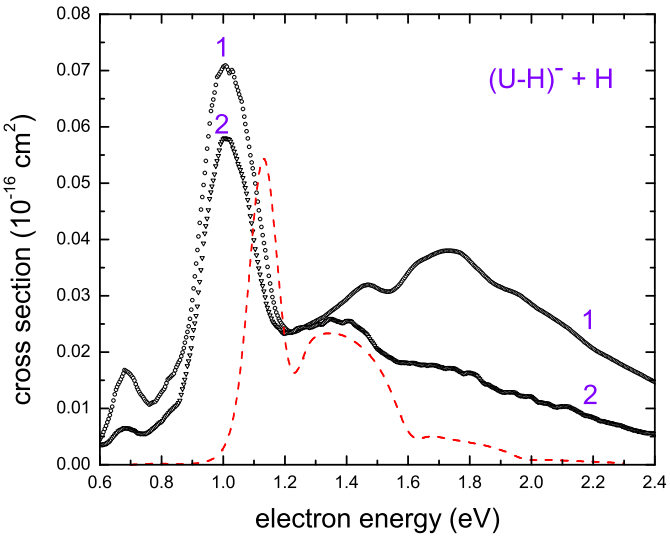

Figure 7 AY10442 16Dec2010

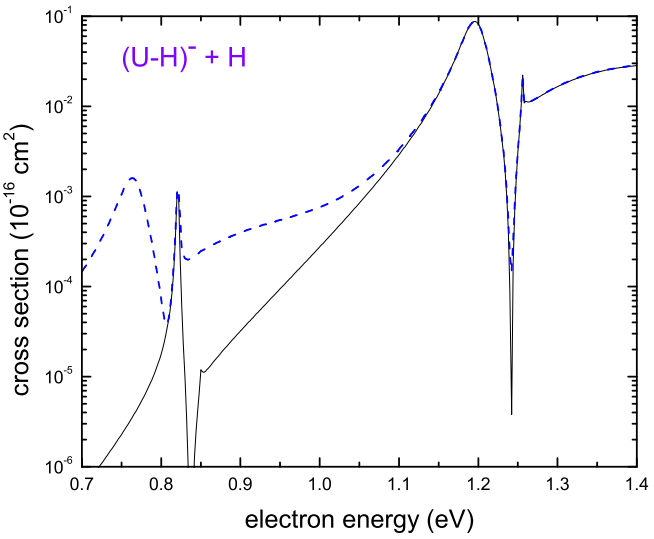

Figure 8 AY10442 16Dec2010

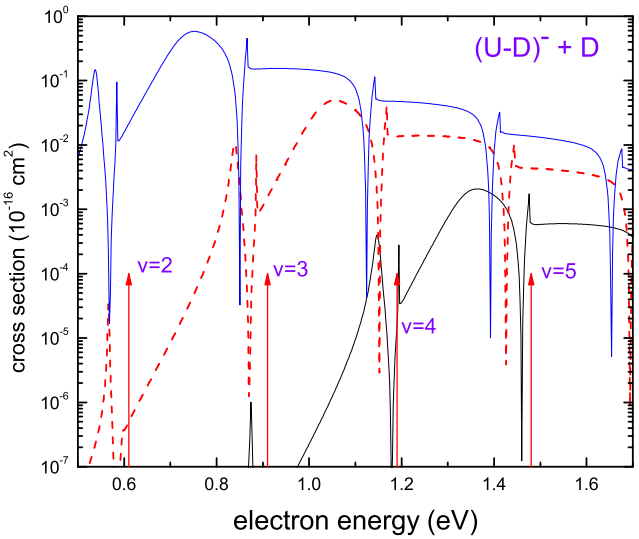

Figure 9 AY10442 16Dec2010

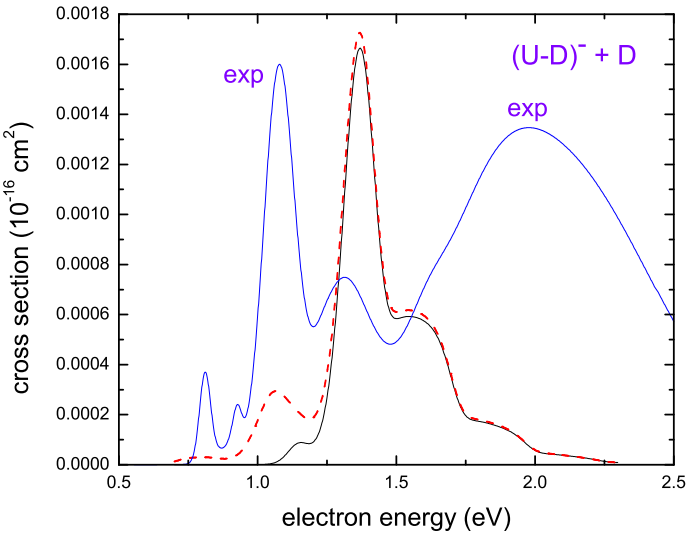

Figure 10 AY10442 16Dec2010

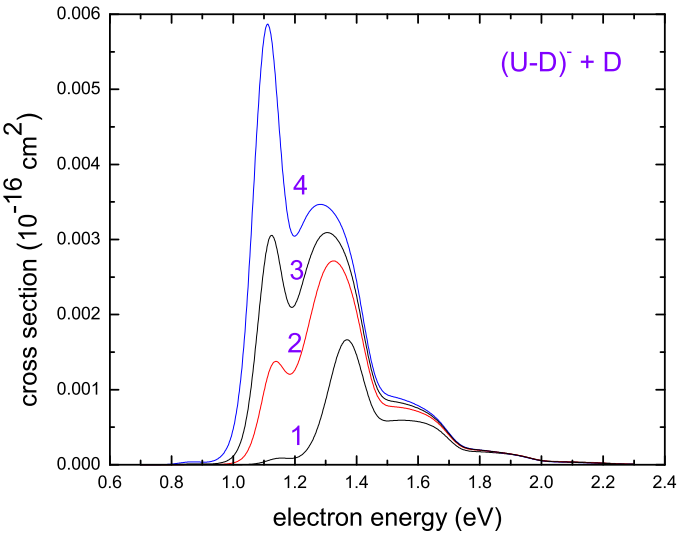

Figure 11 AY10442 16Dec2010